INTRODUCTION TO CELL CYCLE ANALYSIS

Written by
Dr. Peter Rabinovitch, M.D., Ph.D.
Published by
Phoenix Flow Systems, Inc.
6790 Top Gun St. #1
San Diego, CA. USA 92121
858 453-5095
fax 858 453-2117

This chapter is organized into progressively more advanced sections. Feel free to skip ahead to the level appropriate for your background.

THE BIOLOGICAL CELL CYCLE

Reproduction of cells requires cell division, with production of two daughter cells. The most obvious cellular structure that requires duplication and division into daughter cells is the cell nucleus - the repository of the cell's genetic material, DNA. With few exceptions each cell in an organism contains the same amount of DNA and the same complement of chromosomes. Thus, cells must duplicate their allotment of DNA prior to division so that each daughter will receive the same DNA content as the parent.

The cycle of increase in components (growth) and division, followed by growth and division of these daughter cells, etc., is called the cell cycle. The two most obvious features of the cell cycle are the synthesis and duplication of nuclear DNA before division, and the process of cellular division itself - mitosis. These two components of the cell cycle are usually indicated in shorthand as the "S phase" and "mitosis" or "M".

When the S phase and M phase of the cell cycle were originally described, it was observed that there was a temporal delay or gap between mitosis and the onset of DNA synthesis, and another gap between the completion of DNA synthesis and the onset of mitosis. These gaps were termed G1 and G2, respectively. The cycle of G1 $\rightarrow$ S $\rightarrow$ G2 $\rightarrow$ M $\rightarrow$ G1, etc., is shown schematically in Figure 2.1.

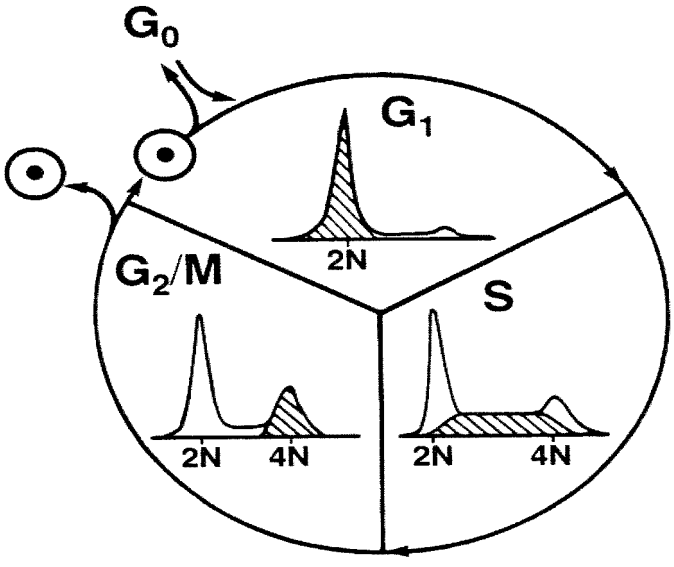

Figure 2.1. *A schematic of the cell cycle, showing flow cytometric components of each phase*

When not in the process of preparing for cell division, (most of the cells in our body are not), cells remain in the G1 portion of the cell cycle. The G1 phase is thus numerically the most predominant phase of the cell cycle and shows up as the largest peak. A subset of G1 cells which are very quiescent and have little of the cellular functions needed to enter the cell cycle are sometimes referred to as G0 cells.

Some of the cellular processes, which take place in the G1 and G2 phases of the cell cycle, are now known. The G1 phase is a synthetic growth phase for many RNA and protein molecules that will be needed for DNA synthesis and cell growth before division. The G2 phase is a time for repair of any DNA damage which has occurred during the preceding cell cycle phases, and for the reorganization of the DNA structure which must take place before the DNA can be divided equally between daughters during Mitosis.

The length of these phases may vary between different cell types that are actively in the process of cell division. Typical time spans in which the cell is engaged in each of the phases of the cell cycle are 12 hours for G1, 6 hours for S phase, 4 hours for G2, and 0.5 hour for Mitosis.

DNA ANALYSIS AND THE

FLOW CYTOMETRIC CELL CYCLE

One of the earliest applications of flow cytometry was the measurement of DNA content in cells; the first rapid identification of phases of the cell cycle other than mitosis. This analysis is based on the ability to stain the cellular DNA in a stoichiometric manner (the amount of stain is directly proportional to the amount of DNA within the cell). A variety of dyes are available to serve this function, all of which have high binding affinities for DNA. The location to which these dyes bind on the DNA molecule varies with the type of dye used.

The two most common categories of DNA binding dyes in use today are the blue-excited dye Propidium Iodide (PI) (or occasionally the related dye, Ethidium Bromide) and the UV-excited dyes diamidino-phenylindole (DAPI) and Hoechst dyes 33342 and 33258. PI is an intercalating dye which binds to DNA and double stranded RNA (and is thus almost always used in conjunction with RNAse to remove RNA), while DAPI and Hoechst dyes bind to the minor groove of the DNA helix and have essentially no binding to RNA. Hoechst 33342 has the distinction of being the only dye presently available which allows satisfactory DNA staining of viable cells. The other dyes require permeabilization of the cell membrane before staining, most often by detergent or hypotonic treatment or by solvent (e.g. ethanol) fixation.

* *Note: Fixation with solvents (e.g. ethanol) often produces considerable aggregation of cells; see subsequent section on analysis of cell aggregation.*

Whichever DNA-binding fluorescent dye is used, a characteristic pattern is seen that reflects the cell cycle phases that make up the mixed cell population.

When diploid cells which have been stained with a dye that stochiometrically binds to DNA are analyzed by flow cytometry, a "narrow" distribution of fluorescent intensities is obtained. This is displayed as a histogram of fluorescence intensity (X-axis) vs. number of cells with each observed intensity. Since all G1 cells have the same DNA content, exactly the same fluorescence should in theory be detected from every G1 cell, and only a single channel in our histogram would be filled (i.e. there would be a very sharp spike in the histogram at the G1 fluorescence intensity, Figure 2.2A).

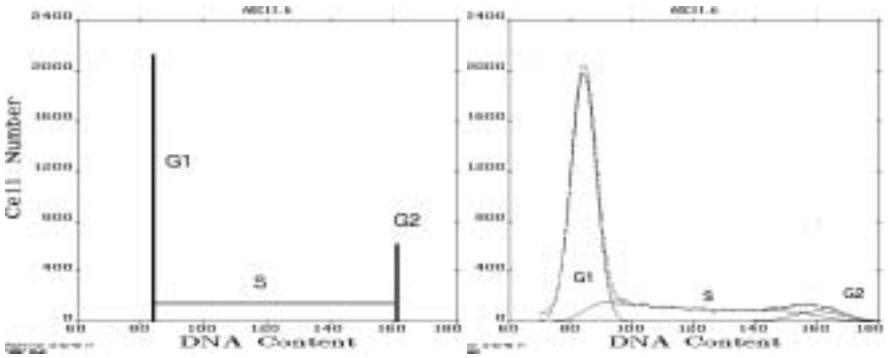

Figure 2.2. *The difference between a histogram from a "perfect" flow cytometer with no errors in measurement (A) and the Gaussian broadening of the histogram that is encountered in all real analyses (B). In B, actual data points are displayed as small diamonds, solid lines indicate the Gaussian G1 and G2 phase components and the S phase distribution, as fit with the Dean and Jett polynomial S phase model. The dashed line shows the overall fit of the model to the data.*

This would occur if the flow cytometer was perfect and if binding of the DNA-specific dye was perfectly uniform. In practice, however, there are a variety of sources of instrumental error in cytometers, in addition to some biological variability in DNA dye binding. Consequently, the measured fluorescence from G1 cells is a normally distributed Gaussian peak. This bell-shaped distribution is characteristic of such variation in measurement (Figure 2.2B).

The greater the observational variation, the broader the resulting Gaussian peak. The term "Coefficient of Variation" (CV) is used to describe the width of the peak. CV is a normalized standard deviation defined as CV = 100 * Standard Deviation / Mean of peak.

Similarly, G2 and mitotic cells, described as having twice the normal G1 DNA content, produce a Gaussian peak in the DNA content histogram with a mean position approximately twice that of the G1 peak – D.I. 2.0. (see Figure 2.2).

In fact, the G2/G1 ratio is usually less than 2.0, due to the fact that the DNA-protein (chromatin) packing is tighter or more condensed in G2 cells than in G1 cells. Consequently, the DNA binding dyes usually have slightly impaired accessibility to their DNA binding sites. A G2/G1 ratio of about 1.97 is more common.

In a theoretically perfect flow cytometer, S phase cells would be observed in the histogram starting just above the position occupied by all the G1 cells, and some of the S phase cells would be found in each channel extending up to just below the position of all the G2 cells. As cells first begin to synthesize DNA in the S phase they have a DNA content just barely above their starting G1 content. The DNA content increases progressively until they complete the S phase with the G2 DNA content.

Unfortunately, the histogram is not so simple, because the same factors, which broaden the G1 and G2 peaks also, broaden the S phase distribution. This results in early S phase cells overlapping with G1 cells, and late S phase cells overlapping with G2 cells. Accounting for this overlap in order to derive the correct proportions of G1, S and G2 phase cells, is the subject of a succeeding section.

DIPLOID AND ANEUPLOID DNA CONTENTS

As described in the previous section, all G1 cells in an organism, with few exceptions, have the same DNA content and the same chromosomal complement. In mammals, this is two of each chromosome type. This is referred to by cytogeneticists (who actually look at chromosomes) as the “diploid DNA content”, and the designation “2N” is used to describe this value (where N refers to a single complement of chromosomes, the haploid DNA content). Flow Cytometrists usually use the designation “DNA Index (D.I.)1.0” to describe this content.

Other DNA contents are not necessarily abnormal, as S phase and G2 cells have the DNA contents described above, gametes have haploid DNA contents and a few cells in the body have tetraploid (D.I. 2.0) DNA contents (other exceptions are a few types of multinucleated cells). All of these DNA contents are together referred to as “euploid values”, and all share the distinction that the chromosomes are in intact sets and each chromosome is itself an unaltered subunit. Any other DNA content has either an abnormal set of chromosomes or at least one abnormally constructed chromosome and

is referred to as an "aneuploid" (literally other than euploid) DNA constitution.

Since whole cell or whole nucleus DNA flow cytometry does not measure or examine chromosomes, flow cytometry cannot tell whether a cell, which has a DNA Index of 1.0, has a normal chromosomal constitution, and so it should properly be referred to it as "indistinguishable from diploid".

Similarly, a cell with a DNA Index of 2.0 could be a "G2 cell", a tetraploid cell, or an aneuploid cell that has abnormal chromosomes. This is properly termed as a DNA content "indistinguishable from tetraploid".

Flow cytometry can detect changes in chromosomes when a population of cells with a DNA content which is not a multiple of DNA Index 1.0 is observed, as this requires that either the numbers or the composition of chromosome(s) have been altered. Since the term "aneuploid" really implies that chromosomes have been evaluated, when just DNA content has been measured by flow cytometry it should more properly be referred to as "DNA-aneuploid" to signify this fact.

DNA aneuploid cell populations are almost always, but not exclusively, associated with malignant tissues. Exceptions that must be noted are some benign tumors (e.g. endocrine adenomas) and some premalignant epithelial cells (e.g. dysplastic epithelium in ulcerative colitis or colon adenomas).

When a malignancy is distinguishable as DNA-aneuploid by flow cytometry, histogram analysis almost invariably shows a mixture of aneuploid and diploid cells in the tumor. The diploid cells consist of lymphocytes, endothelial cells, fibroblasts and other stromal elements, which are always present to a greater or lesser degree.
Both the malignant and the stromal cells have some subset of cells proceeding through the progressive $G1 \rightarrow S \rightarrow G2 \rightarrow M$ stages (the stromal S and G2 phases are usually much smaller than those of malignant cells) and so a DNA content histogram of an aneuploid tumor usually has two overlapping cell cycles, a complication to the cell cycle analysis, but one which MultiCycle has been especially designed to deal with.

CELL CYCLE ANALYSIS OF DNA CONTENT HISTOGRAMS

DNA content histograms require mathematical analysis in order to extract the underlying G1, S, and G2 phase distributions; methods for this analysis have been developed and refined over the past two decades. Methods to derive cell cycle parameters from DNA content histograms range from simple

graphical approaches to more complex deconvolution methods using curve fitting.

All of the simpler methods are based upon the assumption that the G1 and G2 phase fractions may be approximated by examining the portions of the histogram where the G1 or G2 phases have less overlap with S phase. There are two such approaches. The first is to calculate the area under the left half of the G1 curve, and the right half of the G2 curve, and multiply each by two (i.e. reflecting these about the peak mean); what remains is S phase. The second approach is to use only the center-most portion of the S phase distribution, and extrapolate this leftward to the G1 mean and rightward to the G2 mean. What remains on the left is G1 and on the right is G2. These methods can be reasonably accurate when one cell cycle is present and the histogram is optimal in shape. Both methods assume that the G1 and G2 peaks are symmetrical (DNA staining variability in tissues does not always provide this) and that the midpoint (mean) of each peak can be precisely identified. Because of the overlap of G1 and G2 peaks with the S phase, the mean of these peaks is not always at their maximal height (mode), especially for the G2. If a second overlapping cell cycle is also present, then the overlap of the two cell cycles usually precludes safe use of these methods. In addition, modeling of debris and aggregates is usually not a part of these simpler graphical approaches.

The most flexible and accurate methods of cell cycle analysis are based upon building a mathematical model of the DNA content distribution, and then fitting this model to the data using curve-fitting methods. The most well established model, proposed by Dean and Jett (1974) is based upon the prediction that the cell cycle histogram is a result of the Gaussian broadening of the theoretically perfect distribution (Figure 2.2). The underlying distribution can be recovered or "deconvoluted" by fitting the G1 and G2 peaks as Gaussian curves and the S phase distribution as a Gaussian-broadened distribution. As originally proposed, the shape of this broadened S phase distribution is modeled as a smooth second-order polynomial curve (a portion of a parabola, $y = a + bx + cx^2$). The model can be simplified by using a first-order polynomial curve (a broadened trapezoid, i.e., S phase modeled by a tilted line, $y = a + bx$) or a zero-order curve (a broadened rectangle, S phase modeled as a flat line, $y = a$). When the quality of the histogram is less than ideal, especially if G1 or G2 peaks are non-Gaussian (broadened bases, skewed or having shoulders), then the simplified models may give results that are less affected by artifacts that increase the overlap of G1, S, and G2 peaks. This often is the case in analysis of clinical samples, as described in a subsequent section. In this case, a conservative approach is suggested, with a zero, or perhaps first order S phase, unless there is high confidence in the quality of the histogram.

Some experimentally derived S phase distributions (usually from cultured cells) are more complex, and several alternative schemes have been proposed to model such distributions. The most flexible model is that of fitting S phase by the sum of Gaussians (Fried, 1976), in which the S phase is fit by a series of overlapping Gaussian curves. In this model each of the Gaussian curves can be of any height. Therefore, the shape of the S phase is extremely flexible, and this model can fit S phase distributions that have complex shapes. This is also a primary drawback in practical use of this or similar models, however. The very flexible S phase shape allows accurate fitting of any artifacts in the data, and allows increased ambiguity in fitting the region of S near G1 and G2 (i.e., the areas of greatest overlap of G1 and S, and S and G2). A generally successful compromise was suggested by Fox (1980), who added one additional Gaussian curve to Dean and Jett's polynomial S phase model. Fox's model provides a more flexible S phase shape, but still retains the smoothness of the S phase that is characteristic of the Dean and Jett model. It is especially suited to cell cycle analysis of populations highly perturbed or synchronized by drug treatments. Fox's model is available in MultiCycle under the name “Synchronous S” (see Chapter 7).

Curve fitting models are almost universally fit to the histogram data by use of least square fitting. The fitting model is used to generate a mathematical expression, or function, for the predicted histogram distribution. The function has a number of parameters (usually between 7 and 22) that must be adjusted to give the optimum concordance between the fitting model and the observed data. Since the fitting function used by the model is not a simple linear equation, nonlinear least squares analysis is utilized. An excellent description of methods of nonlinear least squares analysis, and sample computer subroutines, is provided by Bevington (1969). The most commonly used technique of nonlinear least squares analysis in these applications is that described by Marquardt (1963). All of the nonlinear least square fitting techniques are *iterative*: successive approximations are made, in which the parameters in the fitting model equations are revised and the fit to the data is successively improved. When no further improvement is obtained, the fit has *converged*, and is theoretically optimal. Goodness of fit is usually quantified by the chi square statistic, $\chi^2 = \sum \frac{(yfit_i - ydata_i)^2}{\sigma_i^2}$, or the reduced chi square statistic, $\chi_\nu^2 = \frac{\chi^2}{\text{degrees of freedeom}}$ which measure the deviation of the fitting function from the data. The speed of the least square fitting is determined by the efficiency in searching for and finding the optimum combination of fitting parameter values. The Marquardt algorithm uses an optimized strategy for searching for the lowest chi square value along the n-dimensional “surface” defined in the space of the chi-square vs. n fitting variables.

An advantage of the least square fitting methods is that the models can be directly extended to analysis of two or even three overlapping cell cycles. The overlapping model components are mathematically deconvoluted to yield individual cell cycle estimates. An additional advantage of curve-fitting methods is that they tend to be less dependent upon the initial or "starting parameters" used to begin the fitting process. Such parameters include initial estimates of peak means and CVs, as well as the limits of the region of the histogram included in the fit. When the cell cycle and debris model is most accurate in fitting the data, the result is least dependent on starting values, and inter-operator variation in results is reduced (Kallioniemi, et al., 1991).

It has been important to recognize that DNA content histograms from tumor tissue are often far from optimal (broad CVs, high debris, and aggregation) or complex (multiple overlapping peaks and cell cycles), and frequently contain artifactual departures from expected shapes (e.g., skewed and non-Gaussian peak shapes). This is even truer when analyses are derived from formalin-fixed specimens. *When a skewed G1 peak or a peak with a "tail" on the right side extends visibly into the S phase, S phase estimates should be used with extreme caution* (Shankey, et al., 1993a).

An important aspect of the analysis of imperfect histograms is the ability to reduce the model's complexity by using simplifying assumptions to reduce the number of model parameters being fit. This may reduce the ability of the model to fit the finer details of a histogram, but it also reduces the possibility of incorrect fitting of the data. As described above, some models may assume that a skew or broad base in G_0 or G_1 peaks is part of the S phase, which can lead to an overestimation of the true S phase. More conservative models may be more accurate in situations where CVs are wide or peaks are not well resolved, when multiple peaks are extensively overlapping, or when background aggregates and debris is high. These situations are more fully described in later sections. The Dean and Jett algorithm may be used with a zero (broadened rectangle), or first order S phase polynomial (broadened trapezoid), instead of the more flexible, but error-prone second-order polynomial. Additional constraints can be imposed to require that the CVs of the G2 and G1 peaks be equal (they are usually very similar), or the CVs of DNA diploid and aneuploid peaks can be made equivalent, or the G2/G1 ratios can be constrained to have a user-supplied value, based upon past laboratory experience. Please refer to Chapter 8 - Fitting Options, for additional information on these alternatives.

Finally, as described below, especially careful attention to fitting of the background aggregates and debris is also required in order to maximize the reliability of cell cycle analysis of complex histograms.

FITTING OF BACKGROUND "DEBRIS" AND EFFECTS OF NUCLEUS SECTIONING

Almost all cell or nuclear suspensions analyzed by DNA content flow cytometry contain some damaged or fragmented nuclei (debris) resulting in events, usually most visible to the left of the diploid G1, which are not fit by the G1, S or G2 compartments. In samples that are derived from fresh tissues or cells, most of these "debris" signals are at the left side of the histogram and fall rapidly to baseline. In the best case, the debris signal is insignificant in the portion of the histogram occupied by the cell cycle. Unfortunately this is often not the case, and it becomes very important to include modeling of the debris curve in the computer analysis in order to subtract the effects of the underlying debris from the cell cycle fitting.

The conventional assumption in debris fitting is that the rapidly declining background debris curve can be fit by an exponential function (e^{-kx}). There are two primary reasons why a simple exponential curve does not usually provide an accurate fit:

1) The shape of most debris curves is not actually exponential. It is more common to observe a component that rapidly declines with increasing DNA content and then a portion, which declines more slowly, or plateaus. This more slowly declining portion therefore has a much greater effect upon the cell cycle fitting than is otherwise predicted from an exponential curve.

2) Debris is a result of degradation, fragmentation, or actual cutting of nuclei, and so extends only leftward (to smaller DNA contents) from each DNA content position. Therefore, the shape of the debris curve is dependent upon where the peaks in the DNA histogram are, and the debris cannot be fit independently of the cell histogram. Since the S phase is the lowest and broadest cell cycle compartment in the histogram, S phase calculations are the most effected by both of these considerations.

To illustrate these two points, examine the effects of applying different models to a histogram derived from paraffin embedded tissue (Figure 2.3). Figure 2.3A shows fitting of a simple exponential curve to the debris region left of the G1 peak. This model does not recognize that much of the debris results from fragments of G1 nuclei, and thus it predicts either too much or not enough debris over the S and G2 phase positions, depending on the fitting region selected.

A more sophisticated model of exponential debris is incorporated into MultiCycle. Taking into account that debris components extend only leftward from the DNA curve position the MultiCycle model assumes that each DNA content position is associated with the production of exponential debris which extends leftward from that position. Because of the different

scales from zero to DNA content positions at the left side of the histogram vs. zero to DNA content positions at the right side of the histogram, the exponential curves produced by the former will look "steeper" and those from the latter will spread out over more channels and appear shallower in their rate of decline.

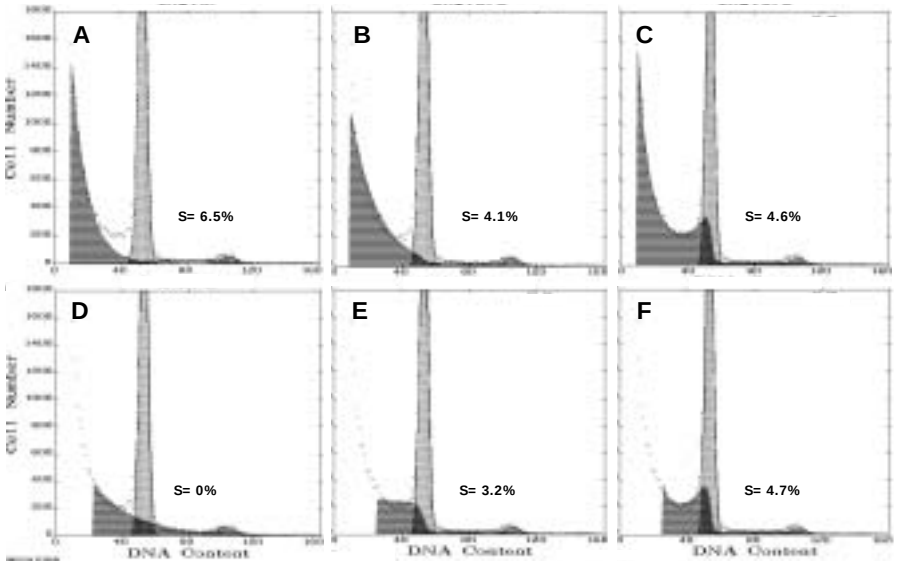

Figure 2.3. *Fitting of a histogram derived from paraffin embedded diploid cells using a simple exponential background debris curve (A), histogram-dependent exponential debris (B), and the sliced nucleus debris model (C). The S phase fraction of the cell cycle analysis is different in each case, as indicated. Simple exponential background debris applied with a left endpoint of the region of fitting that is closer to the G1 peak is shown in (D), resulting in a very different S phase measurement than (A). The histogram-dependent exponential debris applied with the narrower fitting region is illustrated in (E), showing a 22% reduction in S phase compared to B. In contrast, the sliced nucleus model (F) is very insensitive to the change in fitting region.*

Application of this "histogram-dependent" exponential model in MultiCycle is shown in Figures 2.3B and 2.3E. In both cases, the background debris curve drops rapidly from the left side of the G1 peak to the right side of the G1 peak, since the majority of total cells (and thus the source of debris) is in the G1 peak.

Figure 2.3E shows fitting of the debris curve in the region closer to the G1 peak, while 2.3B shows fitting of the region at the lower end of the histogram. Since the debris curve is not actually exponential, different curves are generated for each region chosen for the fit. The S phase estimates also differ – 4.1% for Figure 2.3B vs. 3.2% for Figure 2.3E.

On the positive side, this model yields better results than the simple exponential curve. However, the best fit to this histogram is obtained by use of a model that accounts for the production of debris by the effects of slicing of nuclei by the knife during sectioning from the paraffin block. This model fits all portions of the debris curve, and is therefore much less sensitive to the endpoints chosen for the fitting region as shown in Figure 2.3C and

2.3F. The utility of this model, especially in analysis of paraffin-derived nuclei, is described below.

Analysis of paraffin preserved cells has become an increasingly important part of DNA flow cytometry. Not only is it possible to conduct retrospective research on such material, thereby establishing relationships of flow cytometry results to long-term patient follow up, but in many cases fresh tissue is not available and the analysis of material extracted from paraffin becomes very important in the clinical setting.

In order to derive useful cell cycle information, care must be exercised in the isolation of nuclei and in the computer modeling of the cell cycle analysis. As part of the process of extraction of nuclei from paraffin blocks, sections are usually cut with a microtome at a thickness near 50 μm, and sectioning of nuclei is an unavoidable consequence. These nuclear fragments can have a substantial artifactual effect upon S phase calculations, but a mathematical model of the production of sliced nuclei as part of the cell cycle analysis can help to correct for this effect.

Nuclei in the path of the knife used for sectioning tissue in paraffin blocks are expected to be cut randomly into two portions. If the nuclei were considered in a simple model to be identical cubes randomly cut perpendicularly to one face, then the volume of each randomly cut portion would have an equal probability of being from near-zero to nearly full-volume.

In such a model, a histogram of the volume distribution of a mixture of cut and uncut nuclei would consist of a full-volume peak and a flat continuum to the left ranging from full volume to zero. This is a simplified model of course, but when first introduced in MultiCycle in 1988, it allowed much better fitting of this type of debris than was previously attainable. In fact, it usually requires close inspection of the fitted curves in order to observe the difference between this and the more refined model described in Figure 2.4.

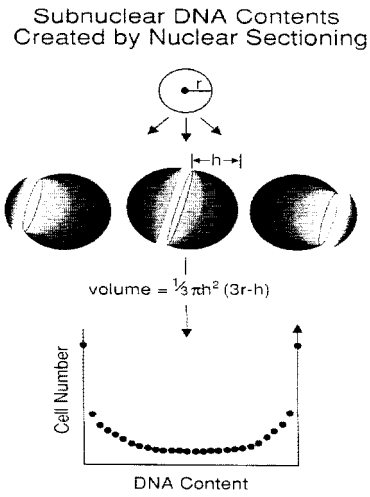

Figure 2.4. *Production of cut portions of nuclei by sectioning with a knife. In the simplest case of spherical nuclei, for a nuclear diameter of "r", if the knife cuts the nucleus at a distance "h" from an edge, then the nuclear volume of this cut section is given by the equation shown. For randomly produced cuts over many nuclei, the theoretical distribution of sizes is shown in the histogram at the bottom (the right*

Since nuclei are actually much closer to spheres or oblate ellipsoids in shape, in a more exact model there would tend to be a somewhat greater fraction of smaller portions produced, as the rounded ends of the nuclei produced "crescents" of smaller volume when cut, and of course, the remaining "halves" would be correspondingly larger portions. A histogram of volumes resulting from random slicing would thus produce a distribution which extended from zero to full-volume, but with a concave rather than a flat distribution, as shown in Figure 2.4. Bagwell et al. (1990) have in fact shown that this "spherical" modeling yields the identical result as that derived for ellipsoids.

This model is implemented in MultiCycle to correct for this effect in background debris analysis. For DNA content distributions resulting from analyses of cycling cells, mixtures of diploid and aneuploid nuclei (or both) the above model of the effects of cutting nuclei can be implemented by considering each channel of the distribution to be a discrete population of DNA contents for which a certain proportion are cut by random probabilities and therefore form a flat-concave continuum to the left of that channel. The probability of a nucleus being cut should be proportional to its radius; in MultiCycle the approximation is made that nuclear volume is proportional to DNA content (e.g., S phase and G2 phase nuclei are larger than G1 nuclei).

Figure 2.5 below (A-I). *Sliced nucleus debris modeling in cell cycle analysis of lymphocytes (A, D, G), HeLa cells (B, E, H) and mixtures of these cells (C, F, I). Analyses were performed on fresh cells (A, B, C), paraffin embedded cells sectioned at 50 microns (D, E, H), and paraffin embedded cells sectioned at 20 microns (G, H, I). The debris component of the fitted model is shown by the horizontally hatched portion, and S phase is diagonally hatched.*

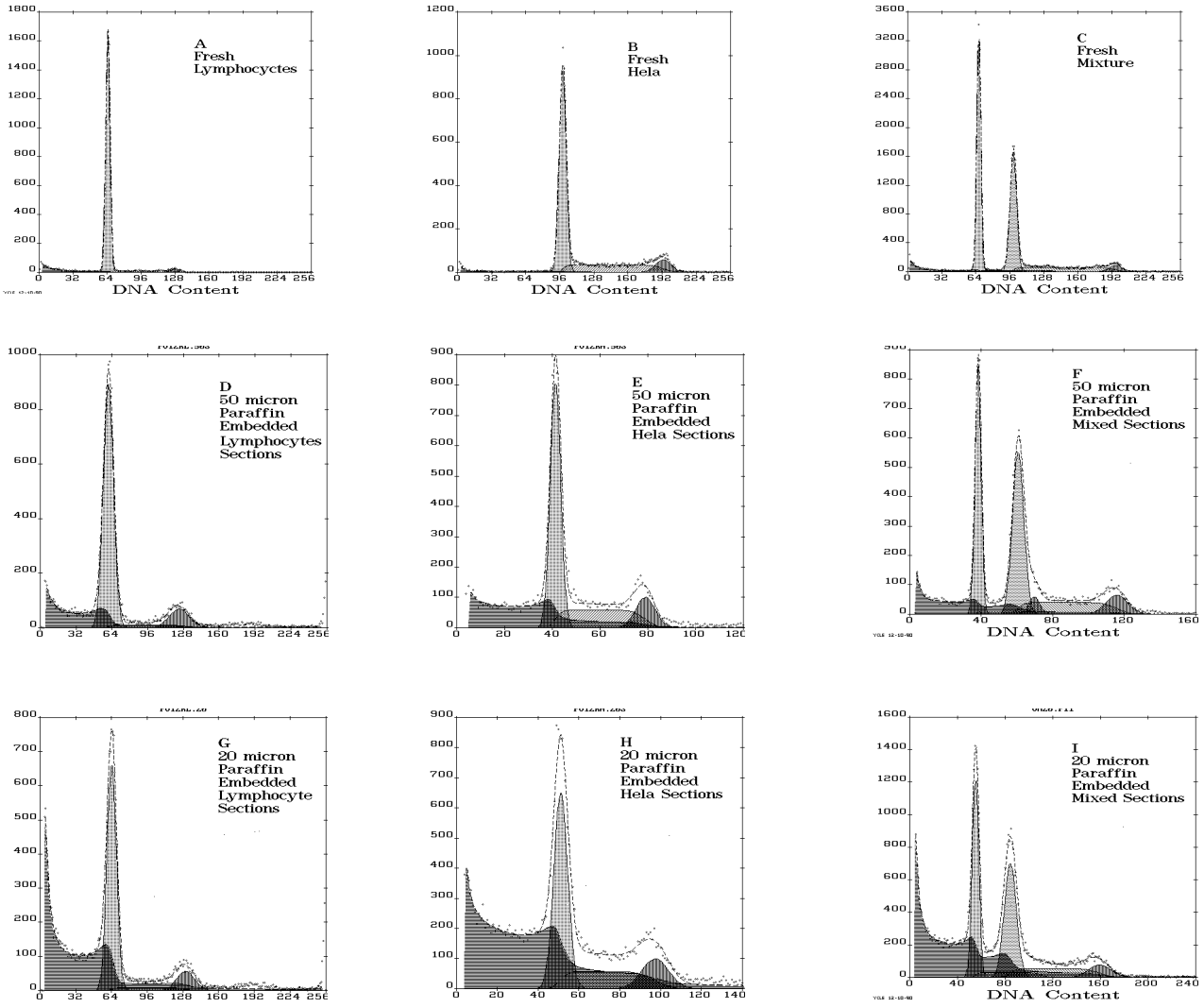

The process of least squares fitting is used to determine the probability of nuclear cutting that yields the best fit to the data. Because small nuclear debris may result from degenerating cells and other fragmentation besides cutting with the microtome, an additional exponential component of the type described previously is also added to the "background" distribution, primarily influencing the left-most portion of the histogram fitting.

To illustrate the utility of this algorithm, DNA content histograms from growing human lymphocytes and HeLa cells (derived from an adenocarcinoma) and mixtures of these cell types were examined. The cells were analyzed both fresh and after formalin fixation, paraffin embedding and extraction from paraffin and staining for flow cytometry.

The debris portion of the histograms shown in Figure 2.5(A-I) increases from fresh (A-C) to 50 micron (D-F) to 20 micron (G-I) section thicknesses. The shape of the debris curve to the left of the G1 peak in paraffin-derived samples is indeed not exponentially declining, but contains a broad plateau, as predicted from the model of random sectioning of nuclei.
The ability of the computer model to closely fit this shape is evident in Figures 2.5D through 2.5I. Table 2.1 shows a comparison of S phase estimates with and without fitting of the background debris. In the case of fresh tissue (Figure 2.5A-C) it is not readily apparent (except when the y-axis is magnified) that the shape of the debris curve of the freshly analyzed cells has a flat-concave component, in small amounts (see example file ASCII.2).

For the fresh cells, the effects of the sliced nuclei debris modeling is modest, except for the estimate of the lymphocyte S phase in the sample mixed with HeLa cells (Figure 2.5C, Table 2.1 p 2.16).
In the case of fresh cells, the cut HeLa nuclei overlap the lymphocyte S phase, giving rise to a 3% overestimation of S phase without sliced nuclei debris modeling, and a satisfactory correction of this estimate with the model.

The sliced nuclei model is applicable to the fresh specimens because all cell or nuclear extraction methods for unfixed tissues have some mechanical shearing, often even mincing with a sharp knife or scalpel. Therefore, some component of flat, rather than exponential debris is always observed in histograms from these cells, even if much smaller than that seen in paraffin extracted cells (see below). It is recommended to utilize the sliced nucleus model, even if this shape can only be visualized when the Y axis scale is expanded.

For paraffin-derived lymphocytes and HeLa cells (unmixed), there is an overestimation of both cell's S phases, which increases progressively as the section thickness decreases; this overestimation is almost completely corrected by the debris modeling.

In Figure 2.5, the partitioning of the histogram region between G1 and G2 into both S phase and cut nuclei components can be visualized in panels 2.7D, E, G and H.

When analyzed fresh, HeLa cells showed an S phase fraction of 26%. When the same cells were analyzed after paraffin embedding, but without compensation for effects of nuclear slicing, the S phase fraction was 29 to 34%, depending upon the thickness of sectioning (Table 2.1). This effect on S phase estimation is due to the fact that S and G2 phase nuclei are also cut during sectioning, and some of the cut fragments produced underlie the S phase compartment distribution, adding to its apparent size and altering its shape.

Applying the model for correction yields S phase estimates of 26-27% for both 50 micron and 20-micron sections, closer to the results obtained with fresh cells. Similar results are obtained with cultured lymphocytes (Table 2.1), however because there are fewer S and G2 phase cells, the S and G2 phase corrections are of smaller magnitude.

Much more dramatic effects of nuclear slicing are seen in histograms in which there are two cycling populations with different DNA contents. When lymphocytes and Hela cells are mixed; many of the sliced Hela nuclei overlap the lymphocyte cell cycle distribution and result in an artifactually high estimate of the lymphocyte S phase compartment; this is readily visible in 50 micron sections (Figure 2.5F) and is even more pronounced in 20 micron sections (Figure 2.5I). For these cell mixtures, inclusion of the sliced nucleus model in the cell cycle fitting produces a result which closely fits the raw data, and at both 50 micron and 20 micron section thicknesses the model produces S phase estimates which are closer to that of the fresh cells (Table 2.1), although correction of this effect in 20 micron sections is only partial.

It is also shown in Table 2.1 that the standard deviation of S phase estimates is generally smaller when the debris modeling is applied than when it is not applied (i.e., reproducibility is improved). An additional consequence of the inclusion of the correction for sliced nuclei is that a small part of the breadth of the G1 peak is accounted for by the effect of slicing; at 50 micron section thicknesses the CV of the Hela G1 peak averaged 5.3 without the sliced nucleus model, and 4.7 with the model.

Table 2.1. *S phase estimates (S + S.D.) without and with (in parentheses) sliced nuclei correction (n = 3).*

			Mixed	
	HeLa	Lymphocyte	HeLa	Lymphocyte
Fresh	26.2 ± .4 (25.7 ± .5)	5.5 ± .3 (5.2 ± .3)	27.5 ± .8 (27.7 ± 1.0)	8.7 ± .1 (5.6 ± 0.4)
50 micron paraffin	29.6 ± 2.0 (26.6 ± 1.4)	7.1 ± 1.1 (5.4 ± .7)	33.7 ± 5.0 (28 ± .3)	28.9 ± 2.8 (6.1 ± 2.5)
20 micron paraffin	33.8 ± 1.0 (26.9 ± .8)	12.8 ± 3.8 (6.6 ± 1.1)	43.1 ± 6.8 (31.8 ± 3.8)	41.6 ± 5.8 (18.3 ± 2.6)

In conclusion, the data presented in this section strongly suggests that use of the sliced nucleus modeling will provide more accurate estimates of S phase, especially for paraffin derived cells. The final knowledge of how great an improvement this may be will come from studies performed by the user. Kallioniemi et al. (1991), for example, have found that for node-negative stage I-II breast cancer, the relative risk (RR) of death for high S phase tumors was 3.1 times greater than for low S phase tumors when analyses were made without background subtraction; the prognostic distinction improved to a RR of 4.5 when using MultiCycle's sliced nucleus model. For cancer of the prostate the RR of high vs. low S phase increased from 3.1 to 5.3 using the sliced nucleus model.

FITTING AND CORRECTION FOR THE EFFECTS OF CELL OR NUCLEAR AGGREGATION

In the ideal flow cytometric analysis, a cell or nuclear suspension is free of aggregates or clumps, and the consideration of the cell cycle and debris is sufficient to fit the data. In the majority of "real" histograms, however, careful inspection will reveal evidence of cell aggregation.

"Doublets" of G1 cells will overlie the G2 peak and are difficult to distinguish on the histogram, however triplets will be seen at D.I. 3.0, quadruplets at D.I. 4.0, etc. Not only will the G1 cells aggregate, but S and G2 and nuclear fragments (debris) will also aggregate with G1 cells and with each other. The effects of aggregation are more complex when a sample contains aneuploid as well as diploid cells, as aggregates of diploid and aneuploid cells with each other will occur.

The sources of aggregation can be varied. In some cases disaggregation of tissues will be incomplete and aggregates will remain. Even if disaggregation is initially complete, some preparative procedures for flow cytometry, such as those which employ ethanol or other solvent fixation, or any procedure which uses centrifugation, may reintroduce aggregates.

The conventional approach towards the management of aggregation and its effects has centered on attempts to distinguish aggregates by the altered pulse shape which they may produce when illuminated by a focused laser beam. Subsequent analysis of the DNA histogram is gated on the pulse shape distribution.

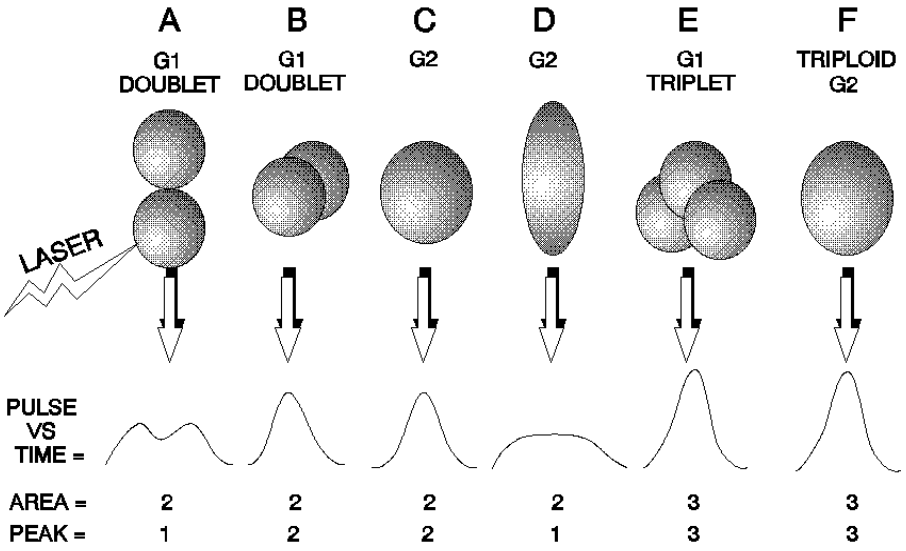

Figure 2.6. *Detection of aggregates on the basis of pulse shape. As cells flow vertically, they pass through a narrow horizontal laser beam. The shape of the pulse of fluorescence intensity vs. time is shown at the bottom. Both the peak height and the area of the pulse can be measured. G1 doublets can pass aligned vertically (A) or horizontally (B). The doublets that pass vertically are distinguished from a round G2 nucleus (C) on the basis of reduced pulse peak. An elongated G2 nucleus (D) may appear similar to (A). A triplet of G1 cells or nuclei (E) may appear indistinguishable from a round triploid G2 (F)*

This approach suffers two notable limitations. First, it requires that the shape of aggregates be different from that of single cells or nuclei. It is easy to imagine that spherical cells or nuclei will appear different from a doublet of two such particles so long as they pass through the laser beam in single file: a G1 doublet produces a fluorescence intensity profile which is twice as long (wide) as that from a single larger G2 (Figure 2.6A vs. 2.6C). However, if the doublet of cells passes through the laser beam with one cell behind the other (Figure 2.6B), then the fluorescence profile cannot be distinguished from that of the G2 cell.

Furthermore, many cells or nuclei derived from solid tissues are themselves oblong, or at least heterogeneous in shape. This is true of most epithelial cells, and malignant epithelial cells (carcinomas) may retain the differentiated shape, or if less differentiated, may be heterogeneous in shape. If an oblong G2 cell passes through the laser beam, then it cannot be easily distinguished from a G1 doublet on the basis of peak or width vs. area (Figure 2.6A vs. 2.6D).

Finally, aggregates of more than two particles can present a problem due to the fact that they may not have a longer axis, and, for example, a G1 triplet

(D.I. = 3) may not be distinguishable from a triploid G2 (D.I. = 3) (Figure 2.6E vs. 2.6F).

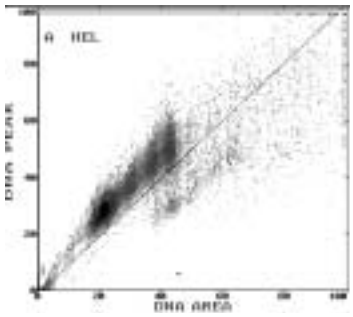

Figure 2.7A

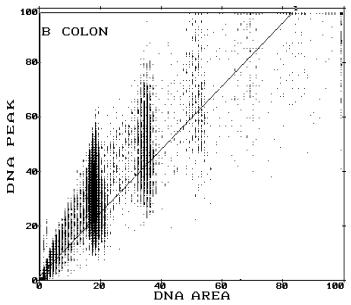

Figure 2.7B

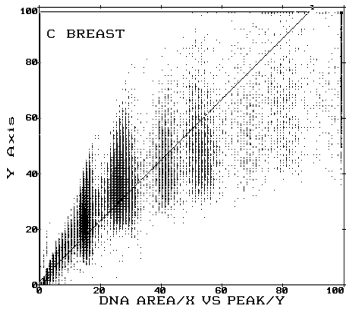

Figure 2.7C

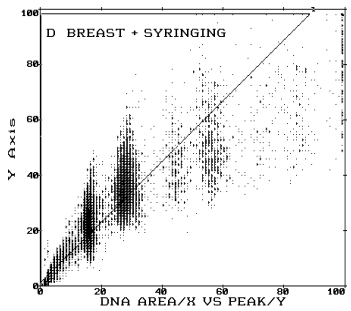

Figure 2.7D

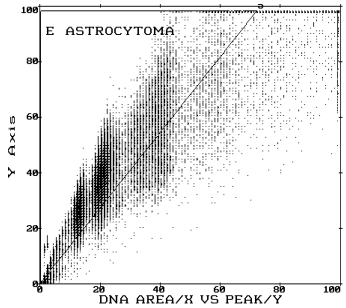

Figure 2.7E

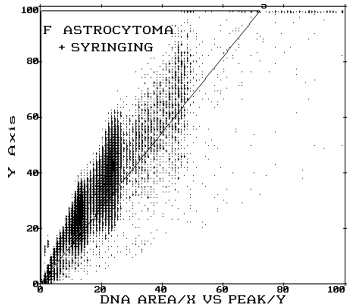

Figure 2.7F

Figure 2.7 (A-F) *shows the application of "doublet" discrimination on the basis of pulse peak vs. pulse area analysis for several cell types. Pulse shape "doublet discrimination" applied to HEL cells (A); colonic mucosal cells (B); nuclei from a breast adenocarcinoma , before (C) and after trituration (D); and nuclei derived from a high-grade astrocytoma, before (E) and after (F) trituration. In each case, the region above the diagonal line was used for gating to attempt to remove aggregates. Further analysis of results is shown in Figures 2.9 - 11. Analyses performed on an Ortho Cytofluorograf with a 5μm high laser beam.*

Figure 2.7A shows fixed HEL cells, a hematopoietic cell with a roughly spherical shape. As with most peak/area analyses, a diagonal line is drawn, with the assumption that aggregates will fall below the line (i.e., their pulse peak value will be lower than non-aggregates for a given pulse area). Figure 2.7A shows that for HEL cells, a large population of doublets does fall below the line, although some particles with DNA content above the G2 value lie above the line and could be undiscriminated aggregates.

Figure 2.7B shows a similar analysis for nuclei derived from normal human colon mucosa minced in a detergent solution. Many of these nuclei are from epithelial cells and are elongated in shape, while some are stromal cells, including lymphocytes, which are more spherical. The distribution of G1 and G2 cells on the plot of peak vs. area is very variable in the peak value, the expected result from the mixture of round and oblong cells.

It is very difficult to see where on this plot the diagonal should be placed in order to exclude aggregates; in essence many of the single epithelial nuclei have the pulse shape of round cell doublets, and doublets of epithelial nuclei may not be formed end-to-end, and thus would not look much different than singlets by pulse shape.

Figures 2.7C and 2.7D show a somewhat more intermediate pattern for analysis of an aneuploid adenocarcinoma of the breast. A diagonal line is shown that does appear to result in most of the G1 triplets and aggregates with DNA content greater than the aneuploid G2 being below the line, and thus excluded from the gated analysis.

Figure 2.7D shows the same cells after trituration by syringing 18 times through a 26-gauge needle. Appreciable aggregation still remains, most below the line, however, as in panel 2.7C, some aggregates appear to remain above the line.

Figures 2.7E and 2.7F show nuclei derived from an aneuploid astrocytoma, before and after syringing, respectively. As for the breast cancer, the diagonal line cannot be placed in a position which appears to exclude all aggregates (without excluding most or all of the G1 nuclei).

Limited attempts to detect aggregates have been made in the past using software. Sometimes this has been attempted by adding an extra peak to the cell cycle model to fit the triplet peak position. This is of very limited utility, since it does not allow for the following:

1) The fitting of much more complicated patterns of aggregation which results from G1, S and G2 interactions, as well as clumping of diploid with aneuploid cells.

2) Compensating for the effects of aggregates which cannot be easily fit as separate peaks because they overlie the cell cycle (including doublets which may overlap G2). This would be possible if one could estimate the proportion of these aggregates based upon the proportions of other aggregates that are better separated and visualized.

In order to allow the software to more completely discern the effects of aggregation, and to compensate for these effects, a theory and model which allows a generalized approach to computer fitting of aggregation in DNA histograms has been developed for MultiCycle.

The basis of the MultiCycle model is the assumption that cell aggregation is, or appears to be, a random event. It is assumed that any two cells or nuclei will aggregate with each other with a certain probability. On the assumption that this probability is the same for all cells, the distribution of doublets, triplets, quadruplets, etc. follows rules, and the net "aggregate histogram" has a characteristic shape which is predicted by random probabilistic aggregation formation.

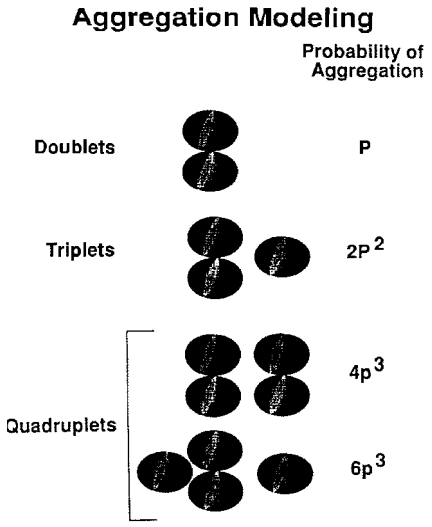

Figure 2.8. *Aggregation modeling by assigning probabilities of aggregate formation to each of the classes of aggregates (doublets, triplets and quadruplets).*

Figure 2.8 illustrates the assumptions made in this model. The basis of this model is the simple assumption that any two particles, i.e., elements of the histogram, have a certain probability of aggregating with each other. Thus, doublets form with a probability p. Triplets form by association of a doublet with a singlet; the singlet can "attach to" either of the 2 cells in the doublet, with a net probability of $2p^2$. Quadruplets can form in two ways: two doublets can aggregate with each other with a probability of $4p^3$ (there are four ways the two doublets can attach to each other, or 4p times p^2), or a triplet can combine with a singlet with a probability of $6p^3$ (three ways to combine the triplet with the singlet, or 3p times $2p^2$).

The constants 2, 4 and 6 are derived here in the simplest fashion; it is quite possible that the "real" constants might be somewhat different. However, from an empirical view, the assumptions above result in a satisfactory modeling of aggregation.

The key to finding the histogram of the distribution of all possible aggregates is to let the computer find all possible combinations of one cell or nucleus with another which can form an aggregate of a particular DNA content. The doublet distribution, D(i), for example, may be mathematically derived from the cell distribution without aggregation, Y(i), by the formula:

$$D(i)= p \cdot \sum_{j=1}^{i} \sum_{k=1}^{i} Y(j) \cdot Y(k) \quad \text{(for all } j+k=i\text{)}.$$

Where Y(i) is the cell distribution without aggregation.
Similarly, the triplet distribution, T(i), is given by:

$$T(i)= 2p^2 \cdot \sum_{j=1}^{i} \sum_{k=1}^{i} D(j) \cdot Y(k) \quad \text{(for all } j+k=i\text{)}.$$

and the quadruplet distribution, Q(i), is given by:

$$Q(i)= 4p^3 \cdot \sum_{j=1}^{i} \sum_{k=1}^{i} D(j) \cdot D(k)$$

$$+ 6p^3 \cdot \sum_{j=1}^{i} \sum_{k=1}^{i} T(j) \cdot Y(k) \quad \text{(for all } j+k=i\text{)}.$$

And, finally, if it is assumed that calculation of aggregates of orders higher than quadruplets is unnecessary (they have only a minimal effect), the net distribution of all aggregates is given by:

$$\text{Aggregates}(i)= D(i) + T(i) + Q(i).$$

Notice that there is only one unknown in the above equations, the value of the probability of aggregation, p.

MultiCycle uses the least squares fitting technique to determine the value of "p" which gives the best fit to the data. The multiple iteration fitting process allows the non-aggregated cell distribution to be determined with progressively improving accuracy as the aggregate distribution derived from the above equations is subtracted from the observed total histogram.

An example of this fitting is shown in Figure 2.9, using the histogram derived from the ungated DNA area analysis of the astrocytoma presented in Figure 2.7E. Note that in 2.9B the events to the right of the aneuploid G1

are fit as part of the aggregate "background", and that the shape of this aggregate distribution is correctly modeled.

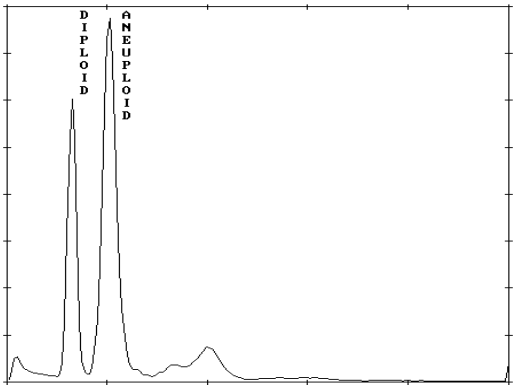

Figure 2.9A

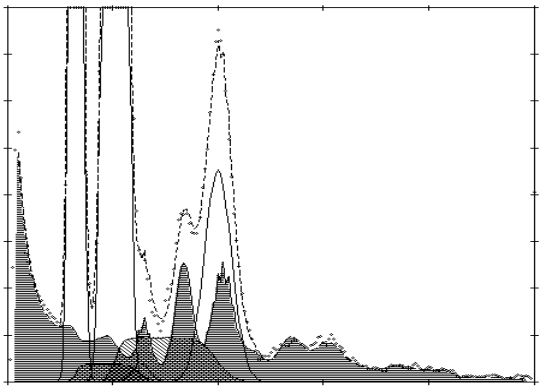

Figure 2.9B

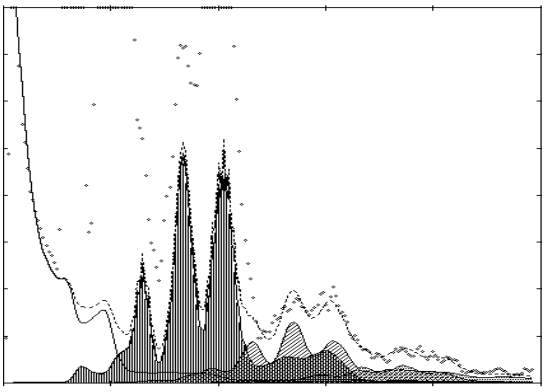

Figure 2.9C

Figure 2.9 (A-C). *Application of the aggregation model to the astrocytoma shown in Figure 2.7C (without gating). Figure (A) shows the raw DNA content histogram. Figure (B) (10X scale) shows the total background fitting (horizontal hatching), including debris and aggregates. Diploid and aneuploid S phases are shown by diagonal hatching, and Gaussian G1 and G2 peaks are shown by solid lines. The total fit is indicated by the dashed line. Figure (C) (20X scale) shows the individual components of the background fit: sliced nucleus debris (solid line at left), doublets (vertical hatching), triplets (diagonal hatching) and quadruplets (stippling). The total background fit is indicated by a dashed line.*

More importantly, however, observe that over the region of the diploid and aneuploid cell cycles the
aggregation background distribution fits several peaks within the histogram, and predicts additional aggregation events in the regions overlying S and G2 phases.

The net result is that there is an excellent fit to the large numbers of peaks in the data (some being due exclusively to aggregation) and additionally, that both S and G2 phase fractions resulting from fitting with this model are lower than if aggregation was not modeled.

Figure 2.9C shows an expanded view of the components which compose the background distribution shown in panel 2.9B. At the left of the histogram, the debris predicted by the sliced nucleus model is seen; this curve declines progressively to the right, as seen previously in Figure 2.5. The doublet distribution (vertical stripes) is seen to be very complex in shape, reflecting the fact that all histogram components (diploid G1, S and G2, aneuploid G1, S and G2) are predicted to aggregate with each other.

It is apparent that this distribution is so complex that to try to model the aggregation peak-by-peak would be impractical. It is a powerful feature of the MultiCycle aggregation modeling that complex distributions are fit as readily as simple ones.

The triplet distribution is shown with diagonal stripes in Figure 2.9C; it has an overall higher DNA content than the doublets, but there is extensive overlap.

There are, in total, fewer triplets than doublets, a consequence of their lower probability of formation. Similarly, the quadruplet distribution is higher in DNA content, and even less abundant than triplets, but overlaps the triplet distribution to a larger extent.

In order to compare the effects on cell cycle analysis of 1) aggregation modeling, 2) pulse processing and gating, and 3) trituration by syringing, the experiments shown in Figures 2.10, 2.11 and 2.12 were performed.

Nuclei were isolated from an adenocarcinoma of the breast (Figures 2.7C and D and Figure 2.10), a high grade astrocytoma (Figures 2.7E and F and Figure 2.11) and normal colon mucosa (Figure 2.7B and Figure 2.12) by mincing in the presence of detergent and DAPI DNA stain. Aliquots of each sample were subjected to either 4 or 18 passages through a 26-gauge needle.

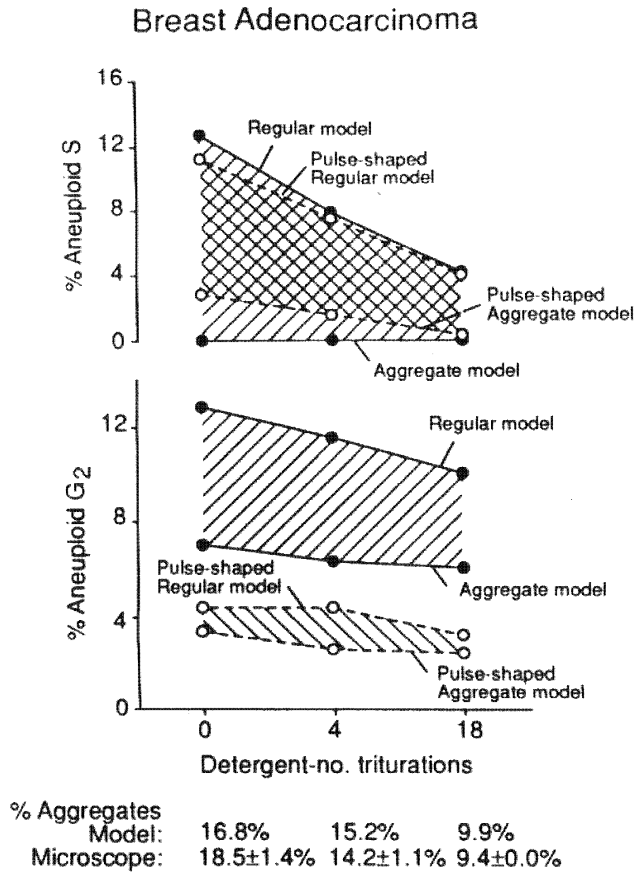

Figure 2.10*. S phase and G2 phase estimates of the aneuploid cell component of an adenocarcinoma of the breast using cell cycle fitting with and without software aggregation modeling, and with and without gating on the basis of pulse shape (hardware "doublet discrimination"). The number of triturations (syringing through a 26-gauge needle) is shown on the bottom axis. The percent aggregates estimated to be present in the histogram by the software model, and the percent aggregates manually estimated by two observers using microscopy are shown at the bottom. Nuclei were isolated by mincing in detergent.*

In addition, whole cells were isolated from the astrocytoma by digestion in collagenase with teasing and mechanical agitation followed by ethanol fixation. Each sample was analyzed as both a gated pulse shape "doublet detected" (above the diagonal in Figure 2.7) histogram and an ungated DNA histogram. Each resulting histogram was analyzed with aggregation modeling and without aggregation modeling (the "regular" model).

For the adenocarcinoma of the breast (Figure 2.10), the S phase of the aneuploid cells without trituration was 12.6%. Gating using the region shown in Figure 2.7C, the S phase was 11.2%. In contrast, the aggregation

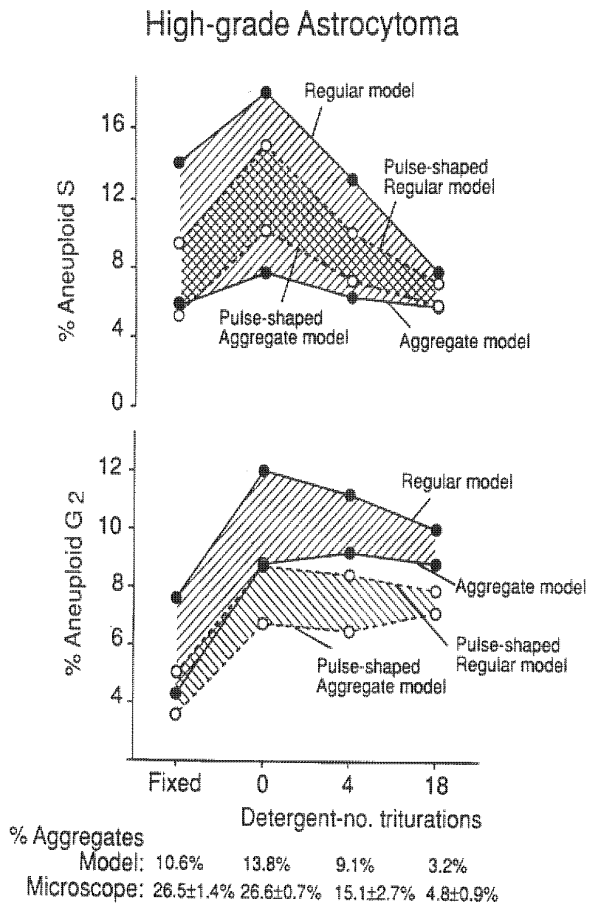

Figure 2.11. *S phase and G2 phase estimates of the aneuploid cell component of a high grade astrocytoma using cell cycle fitting with and without software aggregation modeling, and with and without gating on the basis of pulse shape (hardware "doublet discrimination"). Whole cells were isolated by enzyme digestion and ethanol fixation, and nuclei were isolated by mincing in detergent.*

software model applied to the ungated data reduced the S phase estimate to zero.

The aggregate model calculated that 16.8% of the events were aggregates. Manual counting of aggregates by microscopy (two independent observers) showed a mean of 18.5% aggregates, in good agreement with the software algorithm. Because some of the aggregates were removed in the gated histogram, when the aggregate model is applied to it, the S phase estimate is not reduced as much as in the ungated histogram.

With progressive trituration, aggregation was reduced (software and manual estimates remaining in agreement), and S phase estimates without

aggregation modeling also declined. The estimate with aggregation modeling remained at zero. As microscopy showed that almost half the aggregates were still present after 18 syringings, it seems probable that if further disaggregation of nuclei had been possible, the regular S phase estimate would have declined much further, perhaps also to zero.

The effect on G2 phase estimates, shown in Figure 2.10, illustrates that gating removes substantial amounts of events in the aneuploid G2 position. The aggregate model applied to the ungated histograms shows a reduction also, but not to the level seen in the gated histograms. The aggregation model applied to the ungated histograms yields an estimate which varies only slightly with extent of trituration (syringing).

A plausible interpretation of these results is that gating removes not only some aggregates, but also some legitimate G2 events. Resetting the gating region to remove fewer cells would result in the elimination of even fewer aggregates over the S phase.

A very similar result was obtained with cells from the astrocytoma (Figure 2.11). Trituration was more successful in this example in removing aggregates. The higher estimate of aggregation from microscopic examination may have been due to the presence of cells which visually appeared adjacent but which did not remain aggregated within the flow cytometer. Once again, the software aggregation modeling resulted in an S phase estimate for the aneuploid cells which was almost independent of the degree of aggregation, and was similar for fixed and unfixed cells.

The regular S phase estimate was progressively reduced with trituration. This rate of decline suggests the possibility that had mechanical disaggregation been complete, then the regular model estimate would have equaled the aggregate model estimate. The fixed whole cell preparation appeared to have fewer G2 cells by all estimates. The reason for this is not known, however it is possible that release of G2 cells by enzymatic digestion was less complete than by detergent isolation.

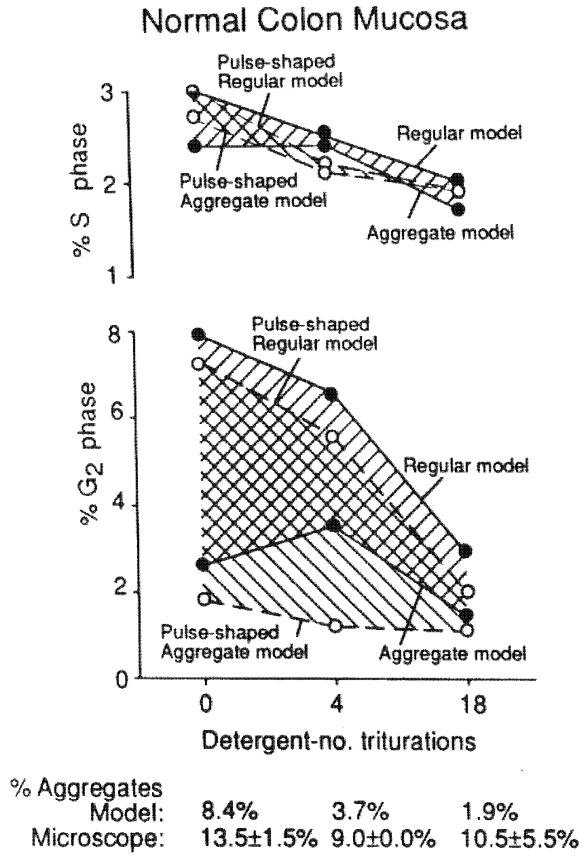

Figure 2.12. *S phase and G2 phase estimates of normal colon mucosal nuclei using cell cycle fitting with and without software aggregation modeling, and with and without gating on the basis of pulse shape (hardware "doublet discrimination").*

Finally, Figure 2.12 shows results obtained with normal colon mucosal cells. These cells have a low S phase. There is not a great difference between any of the models, although there appears to be a slight decline in all S phase estimates with trituration.

The more interesting results with these cells concern the G2 phase estimates. With increasing trituration, a large reduction in the G2 phase is seen in the ungated "regular model". Gating on the basis of pulse shape reduces the G2 estimate by 1%, but does not otherwise change the variation with trituration. In contrast, the software aggregation model shows a lower and more consistent G2 estimate.

In summary, the experiments shown in Figures 2.10-12 demonstrate that, in general, for cell types which have heterogeneous and elongated nuclei, the software aggregation model produces cell cycle estimates that are closer to the values seen in triturated, disaggregated samples.

At present, there is not sufficient data to know whether hardware and software aggregate compensation might in some circumstances be used together (sequentially). Thus, it is suggested that software aggregate modeling be applied to non-gated histograms.

Finally, it should be noted that microscopic enumeration of aggregation requires careful discrimination between merely adjacent vs. adherent cells. Some of the discrepancies between microscopic enumeration and the software estimate could be due to difficulties in distinguishing adjacent from adherent cells. If there is a need to quantify aggregation (even if there is no attempt to compensate for its effects), then the software algorithm may be more consistent. Identification of samples which contain higher amounts of aggregation should allow renewed attempts to triturate and disaggregate the sample, and a repeat of the flow cytometric analysis.

The difference in S phase estimates when applying the aggregation model to clinical samples is suggested by Figures 2.13 and 2.14. In diploid

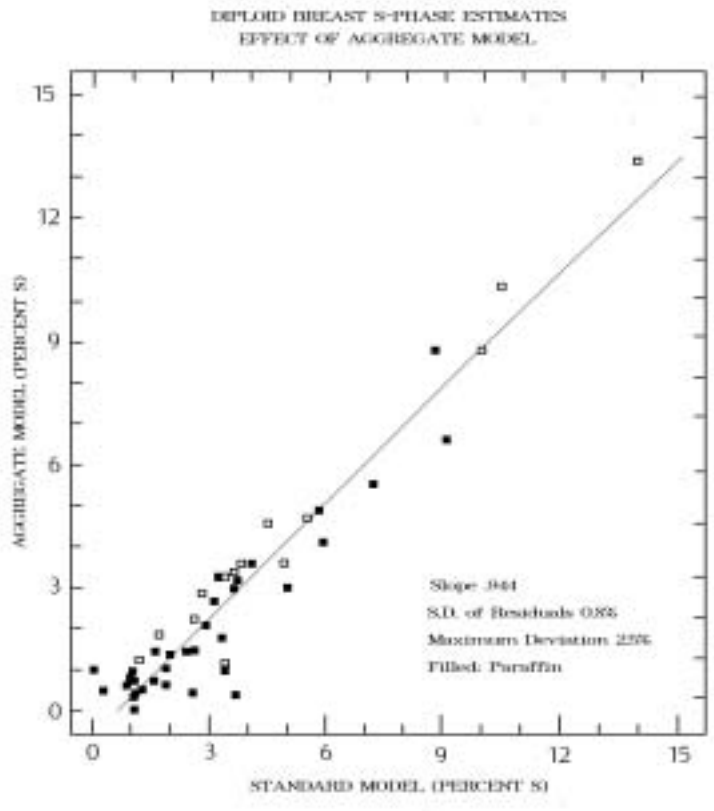

Figure 2.13. *A plot of the S phase values of 47 diploid breast cancers derived from cell cycle fitting using the sliced nuclei model with (ordinate) or without (abscissa) the addition of aggregation modeling. Filled squares are analyses derived from paraffin.*

specimens, fewer aggregates overlie S phase (those that do are primarily aggregates of debris and G1 cells). S phase estimates in diploid breast

cancers were reduced, on the average to 94.4% of the standard model estimate (Figure 2.13), a decline which averaged only 0.89% absolute S phase units, with a maximum decline of 3.4% S phase units. Aneuploid S phase estimates, on the other hand, were reduced to 85.4% of the standard estimate, an average decline of 2.5% S phase units, with a maximum decline of 14.5% S phase units.

Note that in Figure 2.14 there are a number of examples of S phase estimates reduced from the high range (e.g. 13%) to the intermediate range

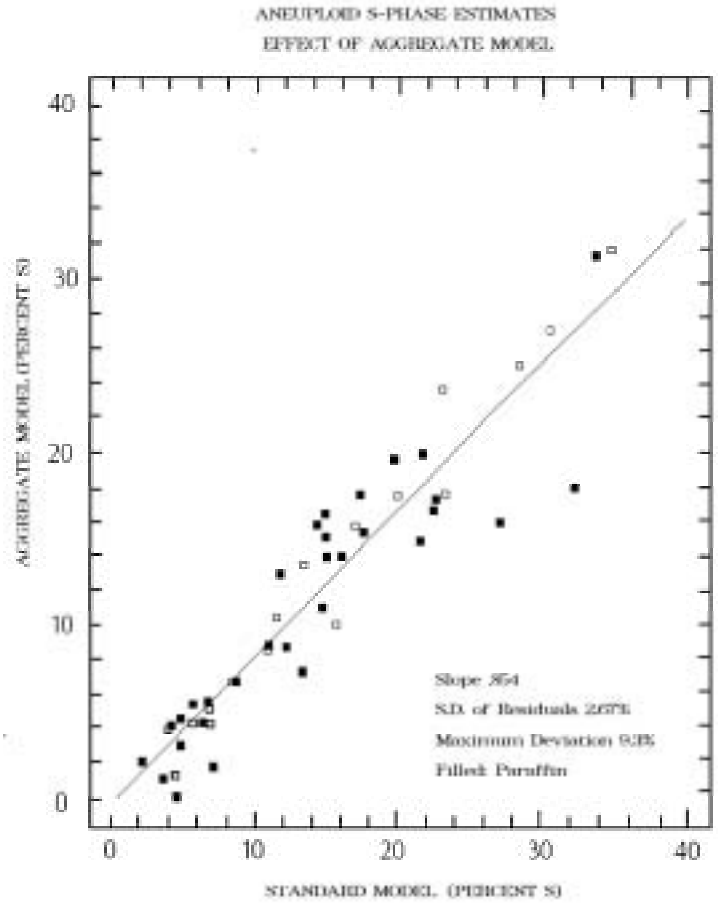

Figure 2.14. *A plot of the S phase values of 56 aneuploid breast cancers derived from cell cycle fitting using the sliced nuclei model with (ordinate) or without (abscissa) the addition of aggregation modeling. Filled squares are analyses derived from paraffin.*

(e.g. 7%), or from the intermediate range (e.g. 7%) to the low range (e.g. 2%).

QUANTITATION OF BACKGROUND AGGREGATES AND DEBRIS

The relative proportion of events analyzed by the flow cytometer that consist of cell or nuclear debris or aggregates is highly variable. The debris is generally higher in paraffin processed tissue, due to nuclear slicing, and in degenerating or necrotic tissue, but these magnitudes are difficult to predict. To address the need for a quantitative measure of aggregates and debris, the DNA Cytometry Consensus Conference defined a parameter termed Background Aggregates and Debris (BAD), defined as the proportion of the histogram events between the leftmost G1 and the rightmost G2 that is modeled as debris or aggregates. The reason that this parameter is defined in this manner, rather than as the total percent debris and aggregates in the entire histogram, is that left and right end-points of a histogram are variable and arbitrary, depending on instrument settings. The proportion of debris in the histogram is especially sensitive to variation in the left limit of data acquisition. The BAD is unaffected by histogram endpoints. It is, however, very much dependent on the choice of histogram modeling. For greatest accuracy and inter-laboratory comparison, it is suggested that histogram-dependent sliced nucleus and aggregation models of background correction be utilized. MultiCycle will calculate and display the % BAD, and will use the BAD as one indicator of cell cycle fitting reliability.

ANALYSIS OF APOPTOSIS

There is increasing interest in measurement of cells undergoing programmed "self-destruction" via apoptosis. During apoptosis, the nuclear DNA is fragmented. The fragments can be removed from cells by one of a number of staining protocols, making apoptotic cells visible as a peak below the G1 DNA content. Usually, this peak is approximately Gaussian in shape and can be quantitated using the "overlapped peak" MultiCycle fitting option.

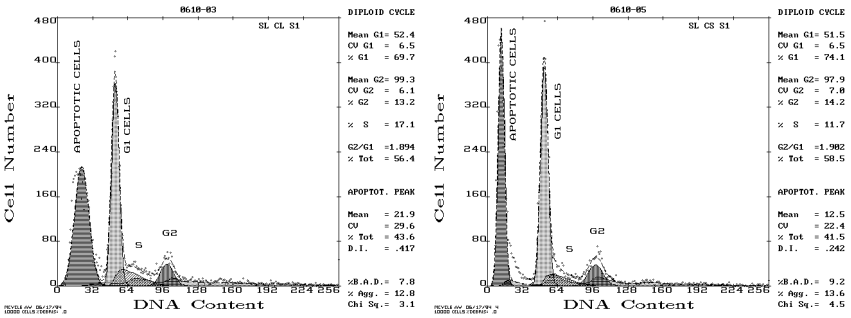

Figure 2.15. *Analysis of Apoptotic populations of cells using the "Overlapped Peak" fitting option. The apoptotic peak in Panel A represents 43.6% of cells, and has 41.7% the DNA staining intensity of diploid cells. In panel B, the cells have been incubated in a more hypotonic buffer, and the apoptotic peak has only 24.2% the staining intensity of diploid cells. Data courtesy of Z. Darzynkiewicz and F. Traganos.*

Figure 2.15 illustrates that the degree of retention of apoptotic DNA fragments within the cell can be influenced by the staining buffer, and that this can be quantitated by histogram analysis. Note that in analysis of apoptotic peaks the lower range limit for peak searching should be set below the apoptotic peak, and the left limit of the debris fitting region should be placed to the left of the apoptotic peak, so that the apoptotic peak is not mistaken for or confused with debris.

BEYOND SINGLE PARAMETER ANALYSIS: DNA VS. IMMUNOFLUORESCENCE

Univariate DNA content analysis offers simplicity of sample preparation, and, with care, accurate cell cycle measurements can be obtained. Considerable future potential, however, will be derived from bivariate analyses, where one parameter is DNA content and the other is an immunofluorescent probe.
In the analysis of solid tissues, important classes of targets for antibody probes will be cell cycle associated antigens, and oncogene products. In order to demonstrate that careful methods of data analysis and cell cycle analysis are still important in this emerging area, an example of analysis of DNA content vs. Ki-67 antibody staining is shown.

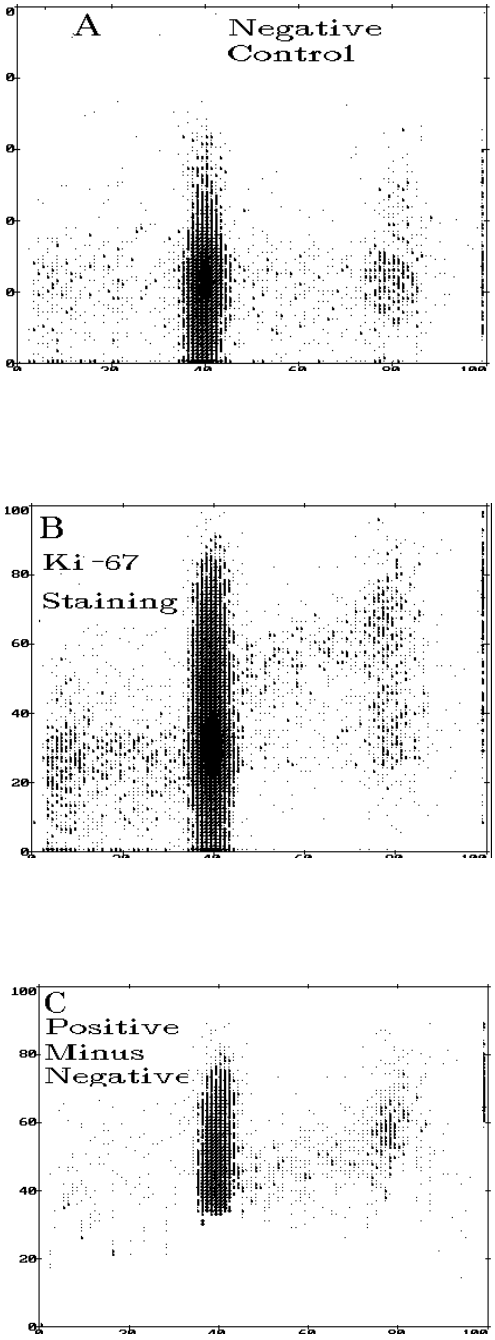

Figure 2.16 (A-C)*. Ki-67 analysis of human Barrett's esophagus. Negative control stained with irrelevant primary and PE-secondary antibody, as well as DAPI DNA stain (A); staining with Ki-67 antibody and PE-secondary antibody vs. DNA (B); and (A)subtracted from (B), shown in (C). The Y-axis is Ki-67 fluorescence and the X-axis is DNA content.*

Figure 2.16 shows the analysis of human esophageal epithelial cells (this example happens to come from metaplastic columnar Barrett's epithelium) with the antibody Ki-67. Expression of the target for this antibody is cell cycle associated: low in quiescent G0 cells and early G1 cells, and higher in late G1, S and G2 cells.

Comparing the negative control (A) with the Ki-67 stained cells (B), one can see that the Ki-67 stained cells have a portion of G1 positive cells, a large proportion of S phase cells positive, and a distinct sub-population of positive and negative G2 cells. The negative "S" phase cells include aggregates of debris and G1 cells, and the negative "G2" cells include aggregated G1 doublets. In order to quantitate the proportion of Ki-67 positive G1 phase cells (activated G1) or Ki-67 positive S phase cells (true S?) one needs to identify positive from negative Ki-67 staining. Merely drawing a line at a point which visually appears to be appropriate has numerous drawbacks, not the least of which is its lack of reproducibility.

An alternative software approach is shown in (C), in which the negative control Ki-67 fluorescence histogram at each interval of the DNA content (X-axis) is subtracted from the corresponding X-axis interval of the positive

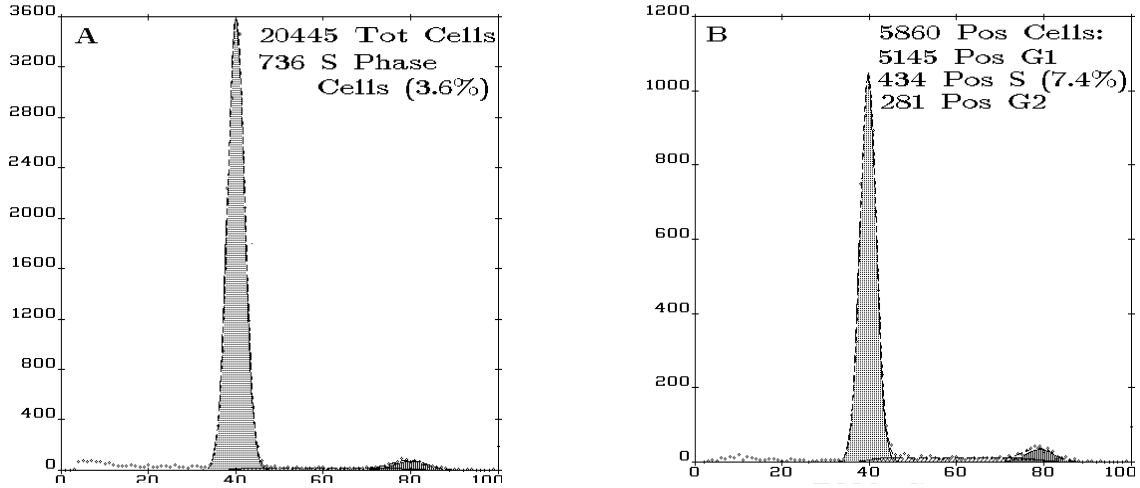

Figure 2.17. *Projections of bivariate data onto the DNA contents X-axis to yield DNA content histograms. Figure A shows total cells from Figure 2.16B and Figure B shows only Ki-67 positive cells from Figure 2.16C. The results of MultiCycle fitting yield the proportions (and numbers) of cells in each cell cycle compartment.*

staining distribution (subtraction is performed using the cumulative subtraction algorithm described by Overton [1988

In order to quantitate the proportion of Ki-67 positive cells in each of the cell cycle compartments, one need only perform a conventional cell cycle analysis upon the X-axis projection of the data, as illustrated in Figures 2.17A and B.

The proportion of total Ki-67 positive cells in each compartment may be calculated by adding into the denominator the Ki-67 negative G1 cells (on the assumption that negative "S" and "G2" cells are artifacts).